PNAS RESEARCH ARTICLE | APPLIED BIOLOGICAL SCIENCES

Type I interferon signaling pathway enhances immune-checkpoint inhibition in KRAS mutant lung tumors

Fernando Fernández-García[a], Ana Fernández-Rodríguez[a], Coral Fustero-Torre[b,1], Elena Piñeiro-Yáñez[b], Haiyun Wang[c], Carmen G. Lechuga[a], Sergio Callejas[d], Rebeca Álvarez[d], Alejandra López-García[a], Laura Esteban-Burgos[a,2], Marina Salmón[a,3], Marta San Román[a], Carmen Guerra[a,e], Chiara Ambrogio[f], Matthias Drosten[e,g], David Santamaría[g], Fátima Al-Shahrour[b], Ana Dopazo[d,h], Mariano Barbacid[a,e,4,5], and Monica Musteanu[e,i,j,4,5]

Affiliations are included on p. 10.

Contributed by Mariano Barbacid; received February 10, 2024; accepted July 5, 2024; reviewed by Julian Downward, Ignacio Melero Bermejo, and Kate D. Sutherland

Lung cancer is the leading cause of cancer mortality worldwide. KRAS oncogenes are responsible for at least a quarter of lung adenocarcinomas, the main subtype of lung cancer. After four decades of intense research, selective inhibitors of KRAS oncoproteins are finally reaching the clinic. Yet, their effect on overall survival is limited due to the rapid appearance of drug resistance, a likely consequence of the high intratumoral heterogeneity characteristic of these tumors. In this study, we have attempted to identify those functional alterations that result from KRAS oncoprotein expression during the earliest stages of tumor development. Such functional changes are likely to be maintained during the entire process of tumor progression regardless of additional co-occurring mutations. Single-cell RNA sequencing analysis of murine alveolar type 2 cells expressing a resident *Kras* oncogene revealed impairment of the type I interferon pathway, a feature maintained throughout tumor progression. This alteration was also present in advanced murine and human tumors harboring additional mutations in the p53 or LKB1 tumor suppressors. Restoration of type I interferon (IFN) signaling by IFN-β or constitutive active stimulator of interferon genes (STING) expression had a profound influence on the tumor microenvironment, switching them from immunologically "cold" to immunologically "hot" tumors. Therefore, enhancement of the type I IFN pathway predisposes KRAS mutant lung tumors to immunotherapy treatments, regardless of co-occurring mutations in p53 or LKB1.

lung cancer | interferon signaling pathway | KRAS | p53 | LKB1

Significance

Restoration of type I interferon signaling in nonimmunogenic KRAS mutant lung tumors alters their tumor microenvironment from immunologically "cold" to "hot," enhancing responses to immunotherapy regardless of co-occurring p53 or LKB1 loss. Our findings, together with ongoing clinical investigation, suggest the necessity of using stimulators of the type I interferon (IFN) pathway to enhance current immunotherapy protocols.

Lung cancer is the leading cause of cancer mortality worldwide, accounting for up to 18% of all cancer-related deaths with the World Health Organization estimating 2.21 million new cases and 1.8 million deaths in 2020. Among lung cancers, lung adenocarcinoma (LUAD) is the most common histological subtype representing around 40% of all lung cancer cases. Most LUADs are diagnosed in advanced stages, which in most cases are incurable diseases (1, 2). Even half of those patients diagnosed at early stages relapse during the following 5 y (3).

About a fourth of LUAD cases contain oncogenic KRAS (Kirsten rat sarcoma) mutations. Early efforts to block KRAS signaling by inhibiting members of the MAPK or the PI3K pathways have failed in clinical trials due to unacceptable toxicities (4, 5). Recently, covalent inhibitors that selectively target the $KRAS^{G12C}$ isoform have been approved by the U.S. Food and Drug Administration (6–8). Despite significant responses, cancer patients quickly develop resistance hampering the clinical efficacy of these inhibitors (9). Indeed, patients treated with sotorasib display overall survivals similar to those achieved by patients treated with classical chemotherapy regimens (10). Moreover, combination of $KRAS^{G12C}$ inhibitors with immune checkpoint inhibitors does not appear to yield synergistic effects and leads to a higher incidence of treatment-related adverse events, mainly hepatotoxicity (11). In addition, selective inhibitors against other oncogenic KRAS isoforms have been already developed (12, 13). Yet, their clinical efficacy is still unknown.

Inhibition of the PD-1/PD-L1 axis has a significant impact on the management of advanced lung cancer, leading to improved survival rates (14). Combinatorial strategies using PD-1 and CTLA-4 checkpoint inhibitors have also had a significant impact on long-term survival of a subset of patients with advanced LUAD (15, 16). Yet, these treatments have only achieved remission rates in about half the patients, rarely including complete remissions. Moreover, most of the patients develop resistance to these treatments (15–17). Up to date, immune checkpoint inhibitors in KRAS mutant cancer have not

Author contributions: F.F.-G., M.B., and M.M. designed research; F.F.-G., A.F.-R., C.F.-T., E.P.-Y., H.W., C.G.L., S.C., R.Á., A.L.-G., L.E.-B., M.S., M.S.R., F.A.-S., and A.D. performed research; C.F.-T., E.P.-Y., H.W., S.C., R.Á., C.A., D.S., F.A.-S., and A.D. contributed new reagents/analytic tools; F.F.-G., C.G., M.D., M.B., and M.M. analyzed data; and F.F.-G., M.B., and M.M. wrote the paper.

Reviewers: J.D., The Francis Crick Institute; I.M.B., Clinica Universidad de Navarra; and K.D.S., Walter and Eliza Hall Institute of Medical Research.

The authors declare no competing interest.

[1]Present address: Max-Delbrück-Center for Molecular Medicine in the Helmholtz Association (MDC), Berlin Institute for Medical Systems Biology (BIMSB), Berlin 13092, Germany.

[2]Present address: Oncology, Medical Department, Lilly España, Alcobendas, Madrid 28108, Spain.

[3]Present address: Asociación Española Contra el Cáncer, Madrid 28045, Spain.

[4]M.B. and M.M. contributed equally to this work.

[5]To whom correspondence may be addressed. Email: mbarbacid@cnio.es or mmustean@ucm.es.

This article contains supporting information online at https://www.pnas.org/lookup/suppl/doi:10.1073/pnas.2402913121/-/DCSupplemental.

Published August 26, 2024.

uniformly provided positive results. Whereas Gianoncelli et al. did not observe significant differences between KRAS mutant and KRAS wild type LUAD patients in either progression-free or overall survival (18), other investigators reported positive outcomes for KRAS mutant tumors in response to immune checkpoint inhibitors (19). Molecular diversity within KRAS mutant LUAD patients offers an attractive biological explanation for such discrepancy in the results (20).

Identification of those events responsible for the early stages of tumor development is likely to provide targeting opportunities that will not be affected by the intratumoral heterogeneity commonly present in advanced tumors. In this study, we have attempted to identify such alterations in genetically engineered mouse (GEM) tumor models driven by *Kras* oncogenes, either alone or in combination with p53 and LKB1 secondary mutations. The identification of the type I interferon (IFN) pathway as a major player in the early stages of these LUAD should provide additional therapeutic strategies against these tumors.

Results

Single-Cell RNA Sequencing (RNAseq) of KRAS Transformed Alveolar Type 2 (AT2) Cells. To identify the earliest events implicated in KRAS-driven LUAD development, we infected *Kras*$^{+/LSLG12V}$;*ROSA26*$^{LSLeYFP/LSLeYFP}$ and *Kras*$^{+/+}$;*ROSA26*$^{LSLeYFP/LSLeYFP}$ mice with adenoviral vectors encoding the Cre recombinase (Ad5-CMV-Cre). Four weeks postinfection, we isolated AT2 lung cells since they are considered the cells of origin of LUAD (21, 22) (Fig. 1*A*). Single-cell suspensions devoid of red blood cells were sorted by Fluorescence-Activated Cell Sorting (FACS). AT2 cells were defined as alive (DAPI^{-}), nonendothelial cells and nonleukocytes (CD31/CD45-APC^{-}), epithelial (EpCAM-PE^{med}), and MHC-II expressing cells [MHC-II (I-A/I-E)-PE-Cy7^{+}]. MHC-II expression has been previously described to be specific of AT2 cells in the epithelial respiratory tract, and it was used to improve lineage purification (23). eYFP^{+} cell sorting ensured that all the isolated AT2 cells were infected with the Cre expressing adenoviral particles (Fig. 1*A* and *SI Appendix*, Fig. S1 *A* and *B*). As expected, the percentage of eYFP^{+} KRAS wild type AT2 cells (~2%) was significantly lower than those eYFP^{+} AT2 cells expressing the KRAS^{G12V} oncogene (~50%) (*SI Appendix*, Fig. S1 *A* and *B*).

KRAS wild type (223) and KRAS^{G12V} mutant (335) cells were successfully captured and submitted to single-cell RNAseq (scRNAseq). After the filtering process, 315 cells were used for further analyses, including 139 KRAS wild type (*Kras*$^{+/+}$;*ROSA26*$^{eYFP/eYFP}$) and 176 mutant (*Kras*$^{+/G12V}$;*ROSA26*$^{eYFP/eYFP}$) AT2 cells. The average sequencing depth (library size) was around 100,000 reads per cell and the average of detected genes was 2,354 genes per cell. After assessing the quality of the samples, we interrogated how many clusters coexisted within the isolated AT2 cells by performing a consensus clustering considering all 315 cells. Our results indicate the presence of only two populations, with an average silhouette width value of 0.98 (Fig. 1*B*). These two clusters correlated with the KRAS wild type cells, on one hand, and with the KRAS^{G12V} mutant cells, on the other; suggesting that the analysis was performed before intratumoral heterogeneity appearance. Consensus clustering showed that the majority of the KRAS wild type cells were grouped separately from the mutant ones (Fig. 1*C*). One of the most significantly down-regulated gene in KRAS mutant cells when compared to KRAS wild type cells was *Ifi27l2a.* Indeed, cluster analysis showed that the expression levels of *Ifi27l2a* discriminate between AT2 cells expressing wild type and mutant KRAS^{G12V} proteins (Fig. 1*C*).

AT2 Cells Expressing Mutant KRAS Show Impaired Type I Interferon Pathway. Next, we interrogated the transcriptional differences between KRAS wild type and KRAS mutant AT2 cells to identify those pathways affected upon KRAS^{G12V} expression. We used PAGODA2 software to explore pathways and to perform gene set overdispersion analysis with the aim of identifying different aspects of heterogeneity based on transcriptional signatures. We found three aspects of transcriptional heterogeneity associated to

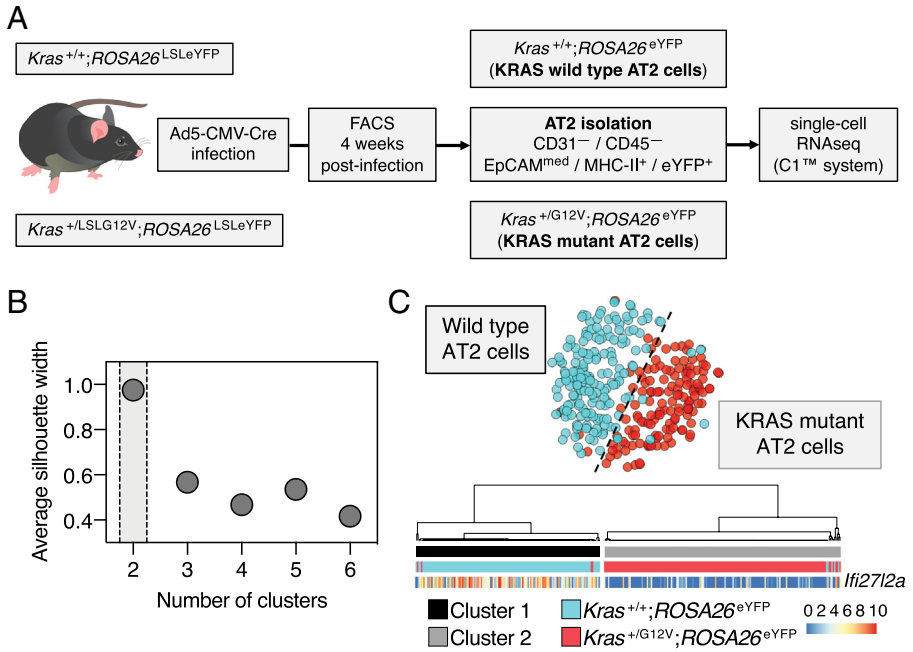

Fig. 1. scRNAseq data reveal two cell populations that differentiate KRAS wildtype from KRAS^{G12V} expressing AT2 cells. Three mice per group were used for AT2 cell isolation prior to scRNAseq. (*A*) Schematic representation of the experimental design. (*B*) Silhouette plot. Indicates the presence of two different clusters (k = 2). (*C*) t-SNE plot and consensus clustering. Most of the KRAS wild type AT2 cells (*Kras*$^{+/+}$;*ROSA26*$^{eYFP/eYFP}$) were grouped in cluster 1, while the KRAS mutant AT2 cells (*Kras*$^{+/G12V}$;*ROSA26*$^{eYFP/eYFP}$) were grouped in cluster 2. Consensus clustering for *Ifi27l2a* follows a red-yellow-blue (high-neutral-low) palette to represent *Ifi27l2a* expression levels from red (high values, KRAS wild type AT2 cells) to blue (low values, KRAS mutant AT2 cells).

annotated gene sets from Gene Ontology (GO) (Fig. 2*A*). Aspect 1 was directly related to those enhanced pathways expected from the higher proliferative properties of $KRAS^{G12V}$ expressing cells such as increased translation, ribosome biogenesis, oxidative phosphorylation, nucleotide salvage pathway, and RNA metabolism (Fig. 2*A* and *SI Appendix*, Table S1). Aspect 2 mainly reflected the loss of AT2 lineage identity and a decrease in surfactant production upon $KRAS^{G12V}$ expression. This process is explained by the decreased expression of gene sets involved in organelles essential for AT2 cell function and homeostasis, such as lamellar bodies, multivesicular bodies, secretory vesicles, and endosomes; as well as a reduction in the metabolism of crucial molecules involved in the synthesis of pulmonary surfactants such as fatty acids, sterol/steroids, thioesters, and secondary alcohols (Fig. 2*A* and *SI Appendix*, Table S1) (24). Among the differentially expressed genes (DEGs), $KRAS^{G12V}$ expressing AT2 cells had decreased expression of AT2 cell markers such as *Sftpa1*, *Lyz2, Sftpb, Lamp3, Sftpd*, *Fasn, Lcn2, Scd1, or Lyz1*. These cells also had lower expression levels of the *Nkx2-1* (TTF-1) transcription factor, suggesting loss of AT2 lineage identity (25, 26). Additionally, we observed decreased response to

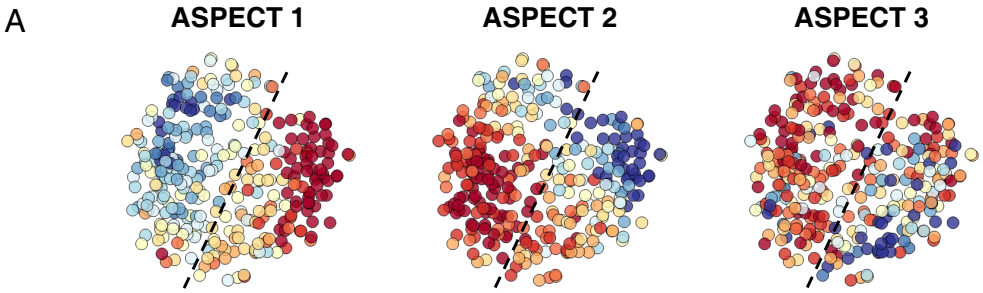

		Gene Ontology	Description	Score
Aspect 1	Gene sets with **increased** expression **in KRAS mutant AT2 cells**	GO:0045047	protein targeting to ER	14,78
		GO:0006364	rRNA processing	14,02
		GO:0006612	protein targeting to membrane	13,89
		GO:0042254	ribosome biogenesis	13,41
		GO:0034470	ncRNA processing	13,12
		GO:0006413	translational initiation	13,04
		GO:0006402	mRNA catabolic process	10,47
		GO:0006119	oxidative phosphorylation	9,28
Aspect 2	Gene sets with **decreased** expression **in KRAS mutant AT2 cells**	GO:0042599	lamellar body	11,00
		GO:0005771	multivesicular body	10,71
		GO:0099503	secretory vesicle	7,75
		GO:0001894	tissue homeostasis	6,99
		GO:0030139	endocytic vesicle	6,75
		GO:0035337	fatty-acyl-CoA metabolic process	6,24
		GO:0008203	cholesterol metabolic process	4,87
		GO:0071277	cellular response to calcium ion	4,74
		GO:0051591	response to cAMP	3,62
Aspect 3		GO:0060337	type I interferon signaling pathway	4,00
		GO:0071357	cellular response to type I interferon	4,00
		GO:0034340	response to type I interferon	3,89

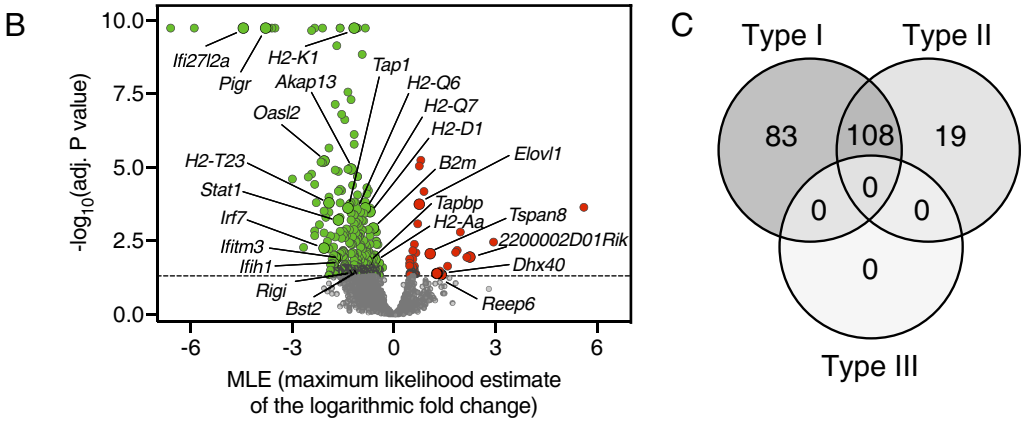

Fig. 2. scRNAseq data reveal three aspects of heterogeneity based on transcriptional signatures. (*A*) t-SNE plots for aspects 1, 2, and 3 are depicted. A red-yellow-blue (high-neutral-low) palette is used to represent aspect scores (cell principal component score). High values (red) correspond to increased expression of associated gene sets and, on the contrary, low values (blue) are related to decreased expression of associated gene sets. Dashed lines delimit $Kras^{+/+}$;$ROSA26^{eYFP/eYFP}$ AT2 (*Left*) and $Kras^{+/G12V}$;$ROSA26^{eYFP/eYFP}$ AT2 cells (*Right*). The table summarizes information about gene sets associated to each aspect of transcriptional heterogeneity. (*B*) Volcano plot highlighting statistically significant IRGs within the DEGs (genes above the dashed line, adjusted *P* value < 0.05), both down-regulated (green) and up-regulated (red) in KRAS mutant AT2 cells relative to wild type AT2 cells. (*C*) Venn diagram showing that most DEGs (334 genes) were considered IRGs regulated by type I and II interferons. The differentially expressed IRGs included in the Venn diagram are listed in *SI Appendix*, Table S2.

cAMP, a property potentially associated to an undifferentiation process (Fig. 2*A* and *SI Appendix,* Table S1) (27).

Aspect 3 revealed decreased response to type I IFN pathway in $KRAS^{G12V}$ expressing AT2 cells (Fig. 2*A* and *SI Appendix,* Table S1). Indeed, most of the DEGs play a major role in the type I IFN pathway (*Stat1*, *Irf7*, *Ifih1*, *Rigi*, *Oasl2*, *Bst2*); as well as molecules involved in antigen presentation (*B2m*, *Tap1*, *Tapbp*, *H2-K1*, *H2-T23*, *H2-Q6*, *H2-Q7*, *H2-D1*, *H2-Aa*) (Fig. 2*B*). In addition, some genes known to be down-regulated upon stimulation with type I IFNs were found up-regulated in $KRAS^{G12V}$ expressing cells (*Elovl1*, *Tspan8*, *2200002D01Rik*, *Dhx40,* and *Reep6*) (Fig. 2*B*). Using the Interferome v2.01 database, we found that nearly 65% of the DEGs (210 out of 334) were interferon regulated genes (IRGs), with around 60% of them (191 out of 334) being regulated by type I IFNs (Fig. 2*C* and *SI Appendix,* Table S2).

Mutant KRAS Is Responsible for Type I IFN Pathway Impairment. To determine whether oncogenic KRAS represses the activation of type I IFN pathway, we expressed a 4-hydroxytamoxifen (4-OHT)-inducible KRAS chimeric protein, ER-$KRAS^{G12V}$, in an immortalized human AT2 cell line and in Calu-3 lung adenocarcinoma cells, which lack *KRAS* mutations. As illustrated in *SI Appendix,* Fig. S2 *A* and *B*, the activation of the $KRAS^{G12V}$ oncoprotein impaired the type I IFN pathway activation induced by RO8191, an IFNAR2 agonist, regardless of whether the cells were of tumoral or normal origin. These observations were confirmed at short time points by the lower levels of pSTAT1 and pSTAT2 upon stimulation with RO8191. Additionally, total STAT1 and STAT2 proteins, which are positively regulated by activation of the pathway, were expressed at lower levels at 8, 24, and 48 h after exposure to RO8191 in the presence of $KRAS^{G12V}$ (*SI Appendix,* Fig. S2 *A* and *B*). In the presence of 4-OHT and therefore active $KRAS^{G12V}$, pERK1/2 levels were higher in starving conditions and ERK1/2 remained activated throughout the experiment (*SI Appendix,* Fig. S2 *A* and *B*). Taken together, these data illustrate that activation of the $KRAS^{G12V}$ oncoprotein results in type IFN signaling impairment. To determine whether these effects could be mediated by changes in type I IFN receptors or their immediate effectors, we analyzed the protein levels of IFNAR1/2 by flow cytometry. In addition, we also measured the expression levels of *SOCS1*, *JAK1,* and *TYK2* by RT-qPCR. As illustrated in *SI Appendix,* Fig. S2*C*, $KRAS^{G12V}$ activation in the AT2 cells induced expression of IFNAR1, while reducing the levels of IFNAR2. Moreover, $KRAS^{G12V}$ did not affect the expression levels of these two receptors in Calu-3 lung tumor cells (*SI Appendix,* Fig. S2*D*). The expression of *SOCS1*, an inhibitor of the catalytic activity of the JAK proteins, was up-regulated in AT2 cells but not in the Calu-3 cells upon $KRAS^{G12V}$ activation (*SI Appendix,* Fig. S2 *C* and *D*). No significant differences could be observed in the expression levels of *JAK1* and *TYK2*, the main effectors of the IFNAR2 and IFNAR1 receptors, respectively (*SI Appendix,* Fig. S2 *C* and *D*). Given that significant differences in IFNAR1, IFNAR2, or *SOCS1* are only observed in AT2 cells but not in Calu-3 cells, we reason that these changes are likely not the cause of a decreased response to type I IFNs upon activation of $KRAS^{G12V}$.

Type I IFN Pathway Is Altered in Early Adenomas. Next, we interrogated whether the impairment of the type I IFN pathway upon $KRAS^{G12V}$ expression was also observed in lesions present at early stages of LUAD development. To this end, we used GEM tumor models of LUAD induced either by expression of $KRAS^{G12V}$ alone ($Kras^{+/LSLG12V}$ mice, K model), or in combination with p53 ($Kras^{+/LSLG12V}$;$Trp53^{L/L}$ mice, KP model) or LKB1 ($Kras^{+/LSLG12V}$;$Lkb1^{L/L}$ mice, KL model) mutations. We harvested by laser capture microdissection small adenomas (300 to 500 μm diameter) at 3 mo postinfection with Ad5-CMV-Cre viral particles in the K model. Due to the shorter latencies observed in the KP and KL tumor models, lesions were harvested from similar adenomas at 6 wk and 5 wk postinfection, respectively (*SI Appendix,* Fig. S3*A*). Adjacent normal alveolar areas of similar sizes from the same mice were used as controls. Principal component analysis (PCA) derived upon RNAseq of these lesions demonstrated that the adenomas obtained from the K, KP, and KL models clustered together, separated from the normal lung samples. These data indicate that at early time points in tumor development, adenomas behave similarly despite having different genotypes (*SI Appendix,* Fig. S3*B*).

Gene set enrichment analysis (GSEA) of the transcriptomic data revealed enrichment of pathways related with the three aspects of transcriptional heterogeneity in lung adenomas (*SI Appendix,* Fig. S3*C*). For instance, several type I IFN–related gene sets were significantly enriched, resembling aspect 3 of transcriptional heterogeneity described above. We observed gene sets related to IFN responses from the Hallmark (Interferon_alpha_response) and the Chemical and Genetic Perturbations (CGP) (Browne_Interferon_responsive_genes or Natsume_Response_To_Interferon_Beta_DN) databases. We also identified other gene sets from the CGP database known to trigger activation of the type I IFN pathway such as those related to DNA damage, adenovirus infection, IFN-β, doxorubicin, azacytidine, and decitabine (*SI Appendix,* Fig. S3*C*). These observations further confirm the impairment of the type I IFN pathway in early adenomas, regardless of their initiating mutational insults.

Type I IFN Pathway Remains Altered in Advanced Murine Lung Adenocarcinomas. Next, we analyzed the expression in advanced LUAD from the K, KP, and KL models of genes that play a major role in type I IFN pathway stimulation (*Rigi*, *Ifih1*, *Stat1,* and *Irf7*), antigen presentation (*B2m*, *H2-T23, H2-Q6*, *H2-K1*, *H2-D1*, *Tap1,* and *Tapbp*), and those significantly down-regulated in KRAS AT2 mutant cells (*Ifi27l2a, Oasl2, Ifitm3*, *Bst2,* and *Sec14l3*) (Fig. 2*B*). 14 out of the 16 genes analyzed by RT-qPCR were significantly down-regulated in all three genotypes of advanced lung tumors when compared to normal lung from *Kras* wild type mice (Fig. 3*A*). Expressions of two genes (*Tap1* and *H2-D1*) were significantly lower only in KP LUAD, while this difference was not significant in K or KL tumors (Fig. 3*A*).

KRAS Mutant Human LUADs Have Decreased Type I IFN Pathway. To determine whether our results could be extrapolated to cancer patients, we used the TCGA database, which incorporates transcriptomic information from human LUAD samples. We retrieved transcriptomic data from 594 samples, of which 59 belonged to adjacent normal lung tissue and 535 to LUAD cases. Within the latter group, 150 samples (28%) presented KRAS mutations. More than one third of these cases (54 cases, 36%) presented KRAS activating mutations in the absence of co-occurring p53 or LKB1 mutations as in the K model; another third (51 cases, 34%) presented p53 alterations as in the KP model, and a fourth (38 cases, 25%) had LKB1 alterations as in the KL model (*SI Appendix,* Table S3). Next, we analyzed the expression levels of the corresponding human orthologs of the differentially expressed IRGs identified by the scRNAseq analysis. Additionally, we included the 22 genes encoding class I and class II HLA molecules. Finally, we explored the expression of 199 IRGs. We found that nearly 40% (75/188) of the down-regulated IRGs in our scRNAseq data were also down-regulated in all K, KP, or KL human tumors. On the other hand, almost 30% (3/11) of the up-regulated IRGs in the scRNAseq data were also up-regulated in all those groups. Around 15% of down-regulated genes were found

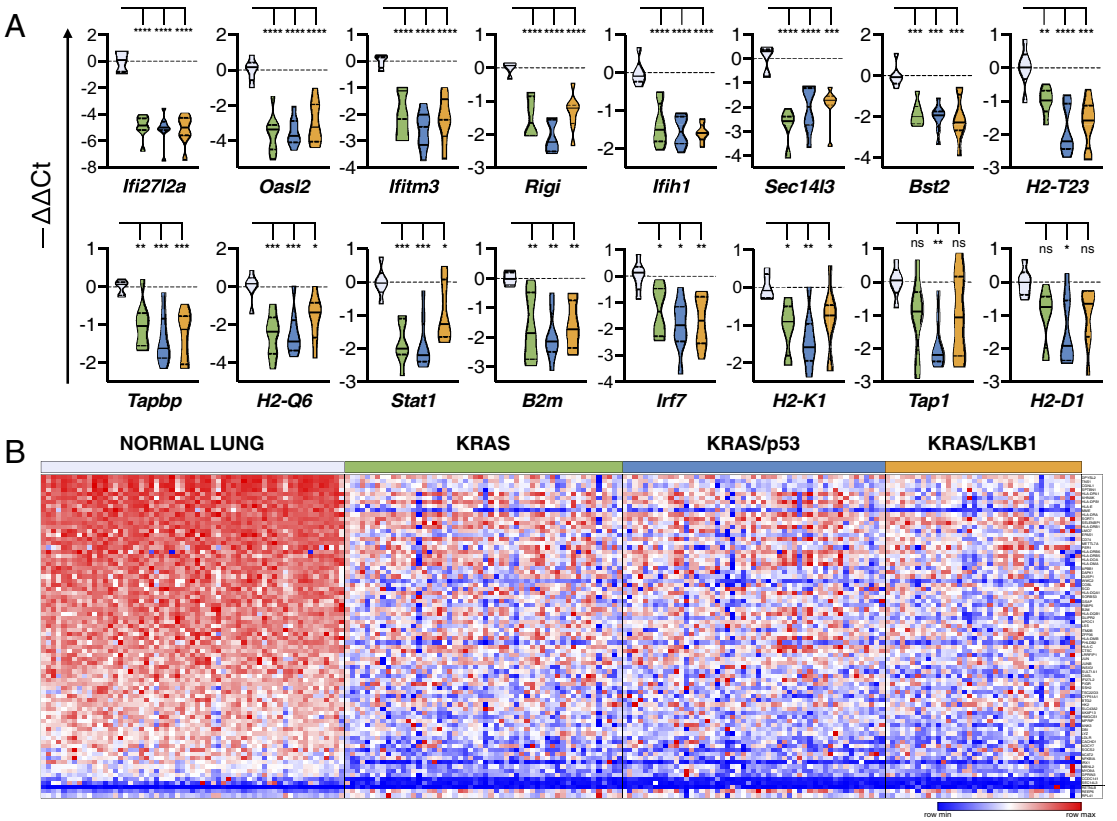

Fig. 3. Type I IFN signaling is altered in murine and human KRAS mutant lung adenocarcinomas. (*A*) Log_2-transformed values of fold changes (−ΔΔCt) of the expression of the indicated IRGs in advanced K (green, n = 8), KP (blue, n = 8), and KL (orange, n = 8) murine tumors compared to the average expression in normal lung tissue from *Kras* wild type mice (gray, n = 6). *Actb* was used for normalization. The violin plot shows density data (shape), median (continuous line), and interquartile range (dashed lines). Plot is truncated in minimum and maximum values. *P* values were obtained by using a Holm–Sidak's multiple comparisons test after one-way ANOVA test to compare groups with a control. ****$P < 0.0001$, ***$P < 0.001$, **$P < 0.01$ and *$P < 0.05$. ns, not significant. (*B*) Heat map showing log_2-transformed values of gene expression (FPKM+1) of significantly down-regulated (75 genes) and up-regulated (three genes) IRGs in human KRAS mutant LUAD carrying the indicated mutations as well as in normal adjacent normal lung tissue. Significance was evaluated using Dunn's multiple comparisons test after the Kruskal–Wallis test to compare the groups with the human normal lung tissue as control. Genes are displayed in rows and squares separate down- from upregulation (upper and lower parts, respectively). A relative color scheme is used in each row. Minimum (blue) and maximum (red) values are used for relative expression. Intermediate expression is colored in white. Patients are distributed in columns, separated in the following groups from *Left* to *Right*: normal lung tissue (gray, n = 59), KRAS mutant (green, n = 54), KRAS/p53 mutant (blue, n = 51), and KRAS/LKB1 mutant (orange, n = 38) tumors. The genes depicted in the heat map are listed in *SI Appendix,* Table S4.

unchanged. Thus, we conclude that an important proportion of IRGs [39%, (78/199)] found dysregulated at early time points in murine tumor cells were also found dysregulated in the same direction in all groups of human LUAD (Fig. 3*B* and *SI Appendix,* Table S4).

Expression of IFN-β and Active STING^{V154M} Induced Upregulation of IFN Response Pathways. Next, we interrogated the effect of restoring type I IFN signaling pathway by expressing IFN-β, a type I IFN cytokine, and a constitutively active mutant form of STING (stimulator of interferon genes, STING^{V154M}) (28). STING is part of the cyclic cGAS–STING–IFN pathway. Briefly, cytosolic DNA is recognized by cGAS, which converts GTP and ATP into cGAMP. This second messenger binds to STING, subsequently activating TBK1 and IKK. These kinases phosphorylate IRF3 and induce the release of NF-κB, leading to the production of type I IFNs and various cytokines and chemokines with proinflammatory functions (29).

We expressed the IFN-β and STING^{V154M} murine constructs in a tetracycline-inducible fashion in mouse tumor cell lines derived from the KP and KL models. Next, we performed RNAseq analysis in these cells after IFN-β and STING^{V154M} expression. PCA demonstrated that KP and KL mutant lung tumor cell lines expressing IFN-β or STING^{V154M} clustered together, separately from non-expressing cells (Fig. 4*A*). In addition, among the most significantly enriched pathways were those related to type I IFN response in both cases (Fig. 4*B*). Upon IFN-β expression we observed a significant increase in the mRNA levels of genes with roles in type I IFN pathway stimulation (*Irf7, Ifih1*, *Stat1*), in antigen presentation (*B2m*, *H2-D1*, *H2-K1*, *H2-Q6*, *H2-T23*, *Tap1*, *Tapbp*) and in those genes significantly down-regulated in KRAS mutant AT2 cells (*Bst2*, *Ifi27l2a*, *Ifitm3*, *Oasl2*) (*SI Appendix,* Fig. S4*A*). On the other hand, STING^{V154M} also stimulates IFN-related pathways by regulating the expression of some of the genes previously mentioned (*Oasl2*, *Irf7,* and *Ifih1*) and other IRGs involved in inflammatory responses and chemotaxis (*Ccl5* and *Cxcl10*), similarly as upon IFN-β expression (*SI Appendix,* Fig. S4*B*).

Stimulation of the type I IFN pathway can induce PD-L1 expression, a well-known inhibitory immune checkpoint (30). Thus, we measured by RT-qPCR the expression of 21 immune checkpoints 48 h after IFN-β and STING^{V154M} expression. We found that in IFN-β overexpressing cells, the top 3 up-regulated immune checkpoints were *Cd274* (encoding PD-L1), *Tnfrsf14* (encoding HVEM), and *Lgals9* (encoding GAL9), with median fold changes of 31.5, 18.2, and 17.6, respectively (*SI Appendix,* Fig. S4*C*). The rest of the immune checkpoints presented a median fold-change less than threefold. On the contrary, the expression of STING^{V154M} did not reveal any significant upregulation of immune checkpoints (*SI Appendix,* Fig. S4*D*). To validate these results at

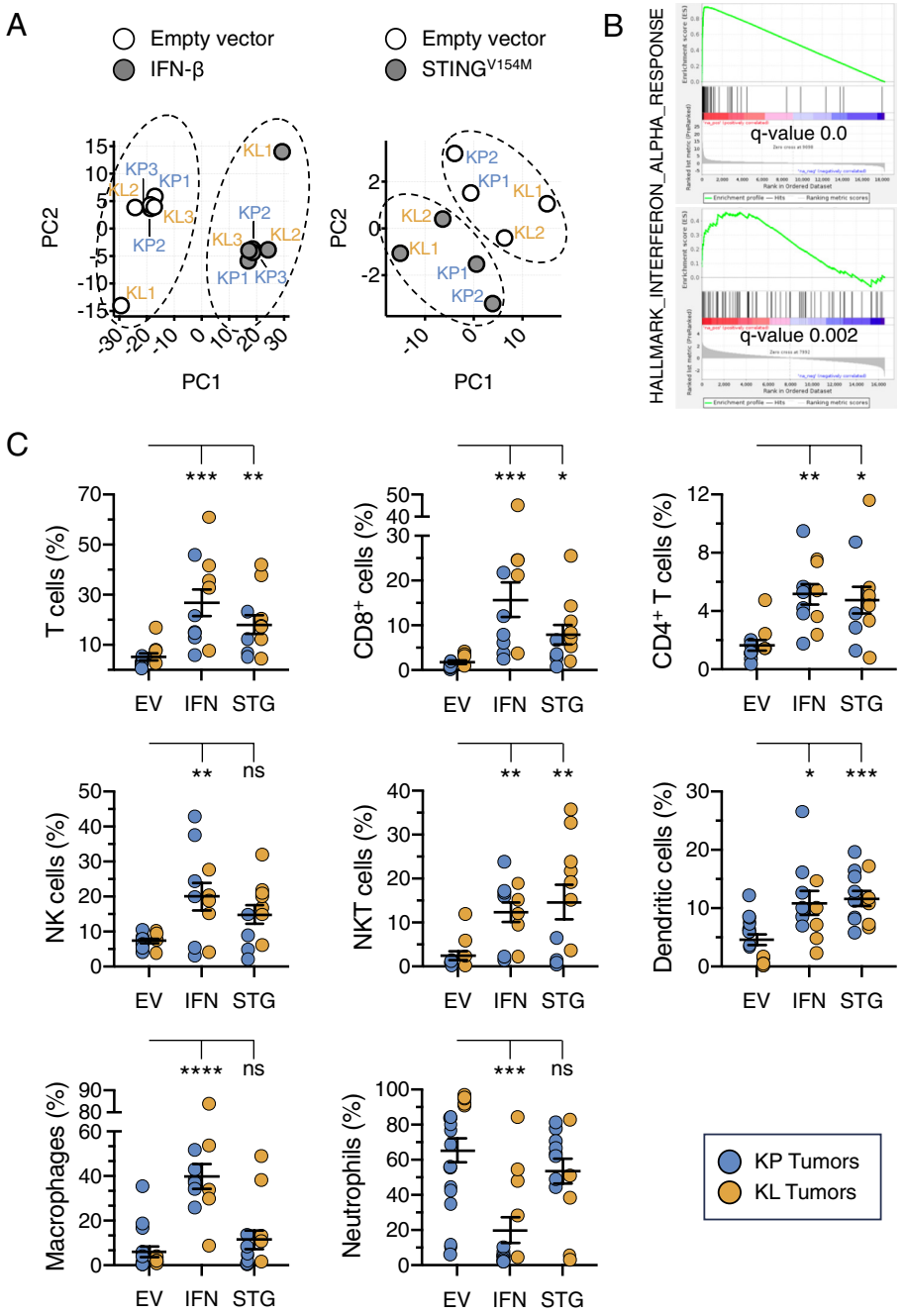

Fig. 4. Expression of IFN-β or constitutively active STING^{V154M} induces enrichment of the type I interferon response and affects the intratumoral immune cell population. (*A*) PCA of RNAseq data from KP (n = 3) and KL (n = 3) tumor cell lines transduced with either empty (open circles) or IFN-β expressing (gray circles) tetracycline-inducible vectors (*Left*) and from KP (n = 2) and KL (n = 2) tumor cell lines transduced with either empty (open circles) or STING^{V154M} expressing (gray circle) tetracycline-inducible vectors (*Right*). (*B*) GSEA for type I interferon response in IFN-β expressing KP (n = 3) and KL (n = 3) cells compared to nonexpressing control cell lines KP (n = 3) and KL (n = 3) (*Top*) and in STING^{V154M} expressing KP (n = 2) and KL (n = 2) cells compared to nonexpressing control cell lines KP (n = 2) and KL (n = 2) (*Bottom*). (*C*) Intratumoral immune cell populations of subcutaneous tumors induced by injection of KP (blue circles) or KL (orange circles) tumor cell lines transduced with either empty (EV), IFN-β (IFN), or STING^{V154M} (STG) tetracycline-inducible vectors after treatment with doxycycline for 14 d were analyzed by flow cytometry immunophenotyping. The percentages of CD3$^+$ T cells, CD4$^+$ T cells, CD8$^+$ T cells, NK cells, NKT cells, and dendritic cells were calculated from the CD45$^+$ cell population. Percentages of neutrophils and macrophages were calculated from the myeloid cell population (CD45$^+$; CD11b$^+$). *P* values were obtained using the Kruskal–Wallis test followed by Dunn's multiple comparisons test. ****$P < 0.0001$, ***$P < 0.001$, **$P < 0.01$ and *$P < 0.05$. ns, not significant. Error bars indicate mean ± SEM.

the protein level, we performed flow cytometry analysis to identify the presence of H-2K^b/H-2D^b MHC class I and PD-L1 surface proteins in the KP and KL cell lines. We confirmed that upon IFN-β induction, the percentage of positive cells for MHC class I alloantigens and their expression levels were significantly increased (*SI Appendix*, Fig. S4 *E* and *F*). Interestingly, whereas nearly all KP tumor cells were positive for PD-L1, only half of the KL tumor cells expressed this protein. Yet, IFN-β expression significantly raised PD-L1 levels in both KP and KL tumor cells (*SI Appendix*, Fig. S4 *E* and *F*). Finally, flow cytometry analysis confirmed that expression of STING^{V154M} did not affect either MHC class I or PD-L1 at the protein level (*SI Appendix*, Fig. S4 *E* and *F*).

KRAS Mutant Tumor Cell Lines Can Be Stimulated Pharmacologically In Vitro to Recover Expression of IRGs. To assess whether loss of IRG expression in KRAS mutant cells could be reverted pharmacologically

we used a reporter assay to measure type I IFN pathway stimulation. K, KP, and KL cells were transfected with a reporter system containing tandem binding sites for IRF7 dimers and the ISGF3 complex followed by a minimal promoter and the nano luciferase cDNA. Two independent clones derived from tumor cell lines obtained from the K, KP, and KL models were stimulated with serial dilutions of RO8191 (an IFNAR2 agonist), poly(I:C) (a TRL3, RIG-I, and IFIH1 agonist) and DMXAA (a STING agonist). IFN-β, a natural agonistic ligand, was used as positive control. The biggest effect was observed upon stimulation of the type I IFN receptor with IFN-β ligand, followed by RO8191 (*SI Appendix,* Fig. S5*A*). Cells were also well stimulated upon poly(I:C) transfection, although with some variability. DMXAA exerted the lowest stimulation potential compared to the rest of the compounds and appeared to be toxic at high concentrations (*SI Appendix,* Fig. S5*A*).

Next, we tested by RT-qPCR whether we could restore the expression of a selection of IRGs. K, KP, and KL cells were stimulated with IFN-β, RO8191, poly(I:C), or DMXAA. As previously demonstrated, the biggest effect was observed when stimulating directly with IFN-β or the IFNAR2 agonist RO8191, both of which induced the expression of all the selected genes in all the cell lines analyzed (*SI Appendix,* Fig. S5*B*). Transfection of poly(I:C) also stimulated the expression of these genes, but the induction was lower than upon IFN-β or RO8191 treatments. DMXAA showed significant gene induction, but only for some of them (*Oasl2* and *Irf7*). Finally, we analyzed the expression of *Cd274*, *Tnfrsf14,* and *Lgals9* (genes coding for PD-L1, HVEM, or GAL9, respectively) in KP and KL tumor cell lines upon stimulation with IFN-β, RO8191, poly(I:C), and DMXAA. We found these three immune checkpoints were significantly up-regulated in all conditions except in the case of DMXAA treatment (*SI Appendix,* Fig. S5*C*).

Expression of IFN-β or STING^{V154M} Changes the Immune Microenvironment of KRAS Mutant Lung Tumors. We also interrogated how the expression of IFN-β or STING^{V154M} alters intratumor immune cell populations in vivo. KP and KL tumor cell lines were transduced with tetracycline-inducible IFN-β or STING^{V154M} expression systems. Subsequently, cells were subcutaneously implanted in the flanks of C57BL/6 immunocompetent mice. Once tumors reached volumes of between 100 and 200 mm^3, mice were fed with a doxycycline-containing diet to induce the expression of IFN-β or STING^{V154M}. After 2 wk, tumors were harvested and processed for flow cytometry immunophenotyping (*SI Appendix,* Fig. S6). IFN-β or STING^{V154M} expressing KP and KL tumors presented a different intratumor immune cell landscape as compared to control tumors showing more infiltration of $CD3^+$ T; $CD8^+$ T; $CD4^+$ T; NK and NKT cells (Fig. 4*C*). The dendritic cell population was also increased in KP and KL tumors upon IFN-β or STING^{V154M} expression (Fig. 4*C*). However, the observed increase in the macrophage cell population and the decrease in neutrophils was exclusively observed upon IFN-β expression (Fig. 4*C*). These results strongly suggest that IFN-β as well as STING^{V154M} expression transforms the immunologically "cold tumors" into immunologically "hot tumors" or T cell-inflamed tumors, which constitutes a requisite for response to immunotherapy treatments (31).

Expression of IFN-β or STING^{V154M} Synergizes with Anti-PD-1 Immunotherapy. Next, we interrogated the effect of anti-PD-1 (α-PD-1) treatment in subcutaneous tumors in the presence of IFN-β or STING^{V154M} expression (Fig. 5*A*). As illustrated in Fig. 5*B*, expression of IFN-β in combination with an α-PD-1 treatment induced a significant antitumoral effect. Such an effect was observed in all biological replicates, regardless of the genotype of the tumors (Fig. 5*B*). α-PD-1 treatment of tumors expressing STING^{V154M} also inhibited tumor growth, albeit to a lesser extent (Fig. 5*C*).

Immunohistochemistry analysis of those tumors expressing IFN-β harvested at the humane endpoint revealed a significant increase in both $CD4^+$ and $CD8^+$ T cells when these mice were treated with α-PD-1, an observation that correlates with the biggest antitumoral effect (*SI Appendix,* Fig. S7 *A* and *B*). KP and KL cell lines either transduced with empty vector or with the inducible IFN-β expressing system were injected subcutaneously in immunodeficient mice as previously described. As illustrated in *SI Appendix,* Fig. S7*C*, tumors expressing the IFN-β cytokine grew at the same pace as nonexpressing tumors. Thus, demonstrating that mature T cells are responsible for the increased therapeutic effect observed upon combined IFN-β pathway stimulation with α-PD-1 treatment. In conclusion, these data indicate that stimulation of type I IFN pathway in KRAS mutant LUAD tumors, independently of the lack of p53 or LKB1, synergizes with α-PD-1 treatment, therefore representing a potential therapeutic strategy against these tumors.

Discussion

The lack of effective therapeutic strategies for KRAS-driven LUAD might be explained by the presence of intratumor heterogeneity in advanced tumors (32, 33). It is widely accepted that those alterations that appear early during tumor development are likely to persist throughout tumor progression and remain present in all tumor cells. Hence, identifying such early alterations that confer fitness advantages during tumor progression could be of interest to find therapeutic strategies that could affect the entire tumor mass. Although both AT2 cells and club cells have demonstrated to yield proliferative lesions in different contexts, AT2 cells seem to be the predominant cell of origin of LUAD upon oncogenic KRAS expression (34). Moreover, scRNAseq revealed that atypical adenomatous hyperplasias from LUAD patients contained cells closely related to AT2 cells (35). Therefore, AT2 cells were considered the cells of origin of LUAD for this work.

scRNAseq analysis of KRAS wild type and mutant AT2 cells revealed a decreased response to type I IFN signaling pathway at very early time points after oncogenic KRAS^{G12V} expression. We observed a reduction in *Stat1*, *Irf7*, *Rigi,* and *Ifih1* expression levels that was maintained in advanced K lung tumors compared to normal lung tissue. Similar results were observed in KRAS mutant tumors that lacked the p53 or the LKB1 tumor suppressors. More importantly, analysis of TCGA database revealed that a decreased response to type I IFNs is also a characteristic of KRAS mutant human LUAD. This impairment of the type I INF response is likely mediated by oncogenic KRAS signaling.

Mechanistically, RAS/MEK signaling has been described to suppress the binding of IRF1 to the promoter regions of viral sensing genes (e.g., *Rigi* or *Ifih1*), and therefore inhibiting their expression (36, 37). Moreover, oncogenic KRAS impairs IFN responses by decreasing the expression of *STAT1*, *STAT2*, *IRF9*, *IRF1,* and *IRF2* (38–41) and attenuating the phosphorylation of STAT1 and STAT2 (40). In this work, we also confirmed a reduced phosphorylation of STAT1 and STAT2 proteins upon type I IFN pathway stimulation in KRAS^{G12V} expressing human AT2 cells and Calu-3 lung adenocarcinoma cells compared to controls without KRAS^{G12V} oncogenic signaling. In addition, mutant RAS can inhibit RIG-I downstream signaling, contributing to reduced IFN-β expression (42). Furthermore, recent studies have

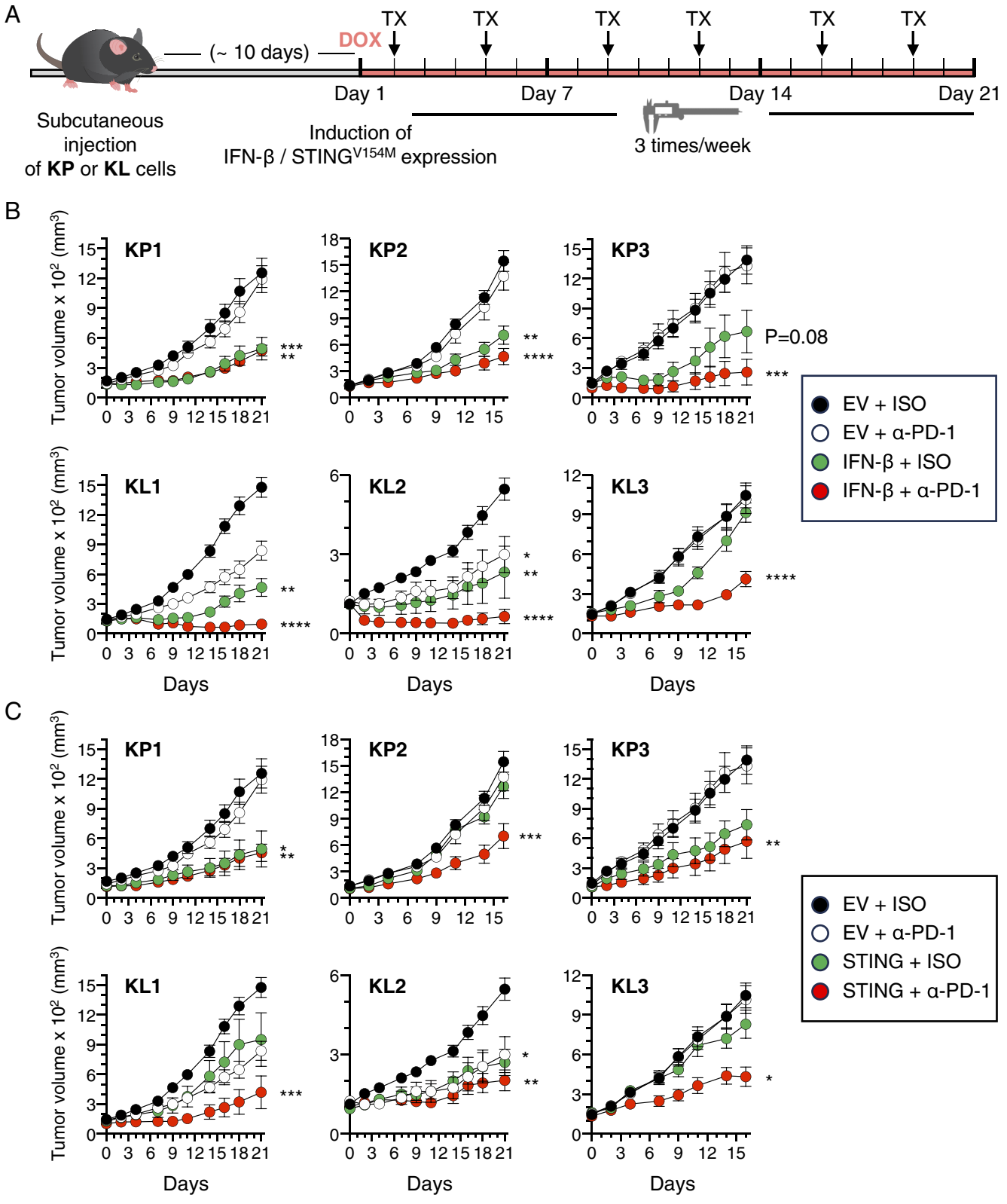

Fig. 5. Expression of IFN-β or STING^{V154M} synergizes with anti-PD-1 immunotherapy. (*A*) Schematic overview of the experimental design. Three independent KP and KL lung tumor cell lines transduced with empty vector (EV) or with a doxycycline-inducible vector that expressed either (*B*) IFN-β or (*C*) constitutively active STING^{V154M} were subcutaneously injected (500,000 cells) in syngeneic mice. When tumors reached volumes of 100 to 200 mm^3 (~10 d post injection), mice were exposed to doxycycline (DOX) and treated with either the IgG2a isotype (ISO) or anti-PD-1 (α-PD-1) antibodies for the indicated time [arrows highlight the days of treatment (TX)]. Mice were randomized into the following groups: (*B*) and (*C*) EV + ISO [solid circles; KP1 (n = 14), KP2 (n = 23), KP3 (n = 19), KL1 (n = 19), KL2 (n = 19), and KL3 (n = 17)], EV + α-PD-1 [open circles; KP1 (n = 14), KP2 (n = 13), KP3 (n = 10), KL1 (n = 12), KL2 (n = 13), and KL3 (n = 17)]. (*B*) IFN-β + ISO [green circles; KP1 (n = 10), KP2 (n = 9), KP3 (n = 9), KL1 (n = 8), KL2 (n = 8), and KL3 (n = 7)] and IFN-β + α-PD-1 (red circles; KP1 (n = 10), KP2 (n = 11), KP3 (n = 10), KL1 (n = 12), KL2 (n = 12), and KL3 (n = 8)]. (*C*) STING^{V154M} + ISO [green circles; KP1 (n = 6), KP2 (n = 5), KP3 (n = 10), KL1 (n = 8), KL2 (n = 8), and KL3 (n = 5)] and STING^{V154M} + α-PD-1 [(red circles; KP1 (n = 7), KP2 (n = 9), KP3 (n = 12), KL1 (n = 7), KL2 (n = 12), and KL3 (n = 6)]. Statistical significance was estimated by calculating the area under the curve for each tumor followed by the Kruskal–Wallis test. Dunn's multiple comparisons test was carried out to compare the five experimental groups with the EV + ISO control group. ****$P < 0.0001$, ***$P < 0.001$, **$P < 0.01$ and *$P < 0.05$. ns, not significant. Error bars indicate mean ± SEM. DOX: doxycycline, TX: treatment.

demonstrated the role of mutant KRAS in down-regulating IRGs expression by upregulation of *MYC* mRNA expression (43, 44).

Avoidance of immune surveillance and cancer immunoediting are major concerns for effective immunotherapy treatments. It has been previously reported that deletion of the 9p21.3 locus, which contains the type I IFN cluster, promotes immune evasion (45). Furthermore, mutant KRAS and subsequent impairment of type I IFN signaling have been associated to an immunosuppressive environment and immune evasion in lung, colorectal, and pancreatic tumor mouse models (39, 43, 44). In the murine tumor scenario, stimulation of type I IFN pathway reverted expression of a battery of IRGs known to play a major role in the type I IFN pathway (*Rigi*, *Ifih1*, *Stat1,* and *Irf7*) as well as molecules involved in antigen presentation (*B2m*, *H2-T23, H2-Q6*, *H2-K1*, *H2-D1*, *Tap1,* and *Tapbp*). Indeed, tumor cell lines derived from K, KP, and KL lung tumor models could be stimulated by expressing IFN-β or $STING^{V154M}$, or by treatment with agonists of the type I IFN receptor such as recombinant IFN-β and RO8191 or the STING agonist DMXAA. Thus, demonstrating that type I IFN signaling can be restored in KRAS mutant cells. Among these strategies, direct IFN-β stimulation restored most DEGs down-regulated in the scRNAseq analysis. However, expression of $STING^{V154M}$ or DMXAA stimulation only induced the expression of some of the selected genes (*Oasl2*, *Irf7,* or *Ifih1*) that play a central role in the type I IFN pathway. These observations indicate that the stimulation of the type I IFN pathway by STING signaling proceeds by different mechanisms, most likely by inducing the expression of *Ccl5* and *Cxcl10*. These genes code for chemokines involved in the recruitment of effector T cells, NK cells, dendritic cells, or macrophages into the tumor, an essential step for immunotherapy success (46).

Despite the fact that GEM lung tumor models closely recapitulate human disease, their immunogenicity does not correspond well with that observed in lung cancer patients. Human KRAS/p53 mutant lung tumors are characterized by an inflammatory response, immunoediting, and expression of immune costimulatory and coinhibitor molecules including PD-L1 (47, 48). Indeed, KRAS/p53 comutations are associated with a potent response, improved progression-free, and overall survival upon immunotherapy treatments (20, 47). On the contrary, inactivating somatic mutations in LKB1 have emerged as a major genomic driver of primary resistance to immune checkpoint inhibitors in non–small cell lung cancer (49). A possible explanation for these differential immunogenic properties between human and mouse tumors might be due to the significantly lower mutational burden of the latter (50). In any case, the fact that the K, KP, and KL mouse tumor models are all poorly immunogenic makes them a valuable tool to determine the molecular bases for their differential response to the immune system. In spite of these general differences, the behavior of one of our KL tumor models resembles the immunogenic features of its corresponding KRAS/LKB1 human tumors. Whereas we do not have an obvious explanation for these observations, we would like to hypothesize that the lack of immunogenicity could be a consequence of its more aggressive proliferative and invasive properties.

Restoration of type I IFN signaling in KP and KL subcutaneous tumor models had an influence on the tumor microenvironment leading to the switch from immunologically "cold" to immunologically "hot" tumors. It has been shown that type I IFNs impact not only on tumor cells but as well as on the response of cells from the innate and adaptive immune system, either directly by stimulating IFNAR1/2 complex or indirectly by inducing the expression of other cytokines/chemokines (51). IFN-α/β promotes the survival of NK cells and enhances their cytolytic functions and IFN-γ production. Moreover, type I IFNs activate dendritic cells, promoting their migration to the lymph nodes and potentiating cross-presentation by conventional type 1 dendritic cells (cDC1), process proven to be essential in immunotherapy (52). Furthermore, type I IFNs directly stimulate $CD8^+$ T cells cell clonal expansion, memory formation, and acquisition of effector cytotoxic functions.

We observed that in our murine models IFN-β and to a lesser extent $STING^{V154M}$ expression were able to promote the infiltration of $CD8^+$ and $CD4^+$ T cells, dendritic cells, and NKT cells. Previous studies have described that STING expression is suppressed upon LKB1 loss, which likely contributes to decreased type I IFN responses in the human KL setting. Moreover, enforced expression of STING led to increased levels of *PD-L1* or *CXCL10* in KL human lung adenocarcinoma cell lines, but this effect was less pronounced in KP cells (53). Although we did not observe changes in the PD-L1 levels upon $STING^{V154M}$ expression, we noted an increased expression of the *Cxcl10* chemokine that could explain the higher T cell content, both in KP and KL murine tumors. Neutrophil infiltration was higher in the KL than in the KP tumors, an observation consistent with previous data indicating that massive neutrophil infiltration, reduced T cell content, and downregulation of MHC-I molecules are features of KRAS/LKB1-driven LUAD (54). Moreover, IFN-β but not $STING^{V154M}$ expression was able to promote a reduction in the content of neutrophils, probably a good prognostic factor due to their immunosuppressive nature (55).

Type I IFNs also induce the expression of proapoptotic IRGs such as TRAIL, FAS, FASL, OAS2, IFI27, IRF3, or IRF7 (56). Furthermore, the p53 gene was shown to be transcriptionally induced by IFN-α/β, resulting in increased protein levels and a boost of p53 response to stress stimuli (57). Although we demonstrated that mature T cells are essential for the observed anti-tumor effects upon IFN-β expression, we cannot exclude a possible contribution of other immune cells or tumor cell-intrinsic functions in such effects, provided that mature T cells are present.

Remarkably, in both KP and KL LUAD tumors, IFN-β-induced type I IFN pathway stimulation or activation of STING along with α-PD-1 treatment had a significant antitumoral effect, indicating that the enhancement of the type I IFN pathway is likely to predispose KRAS mutant lung tumors to immunotherapy treatments.

It is important to emphasize that in this work, we have used a subcutaneous tumor model derived from tumor cell lines that could be easily engineered to overexpress IFN-β and $STING^{V154M}$. We cannot exclude the possibility that the therapeutic effects seen in this model might change when implementing these treatment strategies in endogenous/orthotopic KRAS mutant lung tumor mouse models, where tumor microenvironment would be different. Moreover, further studies should attempt to better mimic human LUAD by using more immunogenic mouse models of KRAS-driven lung tumors (58).

Finally, several clinical trials are currently being conducted to investigate the benefits of using IFN-based therapies in combination with immune checkpoint inhibitors, such as the use of STING agonists (e.g., NCT04096638 or NCT04879849), Toll-like receptors agonists (e.g., NCT05265650), or IFN-β expression systems (e.g., NCT03647163). In summary, our findings, together with ongoing clinical investigation, suggest the necessity of using stimulators of the type I IFN pathway to enhance current immunotherapy protocols.

Materials and Methods

See *SI Appendix, Materials and Methods* for technical details for each method.

Mice. The strains *Trp53*$^{L/L}$ (59), *Lkb1*$^{L/L}$ (60), and *ROSA26*$^{LSLeYFP/LSLeYFP}$ (61) have been described previously. Generation of the *Kras*$^{+/LSLG12V}$ strain was similar to the *Kras*$^{+/LSLG12Vgeo}$ strain described before (62). Animal experiments were approved by the Autonomous Community of Madrid (PROEX 081/16; PROEX 354.0/21). Mice were housed in specific-pathogen-free conditions at CNIO´s Animal Facility (AAALAC, JRS: dpR 001659). Both, female and male mice were used.

Lung Tumor Induction. 8-wk-old mice were anesthetized with a mixture of ketamine (75 mg/kg, Imalgene 1000) and medetomidine (1 mg/kg, Domtor) administered intraperitoneally and a single dose of 10^8 pfu/mouse of Ad5-CMV-Cre (Iowa City, USA) was administered by intranasal instillation. Atipamezole (1 mg/kg, Antisedan) was administered to reverse anesthesia.

Alveolar Type 2 Cell Isolation. AT2 cells were isolated following a slightly modified version of the protocol described by Hasegawa et al. (63).

Single-Cell RNAseq. Isolated AT2 cells were captured using the C1™ high-throughput integrated fluidic circuit (HT IFC). Libraries were prepared using the Illumina Nextera XT DNA Library preparation kit according to Fluidigm's instructions and were sequenced on a HiSeq2500 (Illumina). FastQ files for each sample were obtained using CASAVA v1.8 software (Illumina). The analysis of the scRNAseq data was performed by the Bioinformatics Unit at the CNIO.

Human Tumor Data. For the evaluation of transcriptional differences of the genes of interest in human samples, the data generated by the Cancer Genome Atlas (TCGA) were used, specifically from LUAD and adjacent normal lung samples, available at: https://portal.gdc.cancer.gov/projects/TCGA-LUAD.

RNA Extraction. Lung tumor tissue RNA was extracted using the TRItidy G™ lysis solution (PanReac AppliChem, A4051) and subsequently purified with the RNeasy Mini Kit (Qiagen 74104) following the manufacturer's recommendations. Total RNA from established cell lines was isolated using the RNeasy Mini Kit (Qiagen 74104).

RT-qPCR. Synthesis of cDNA was performed using SuperScript™ II Reverse Transcriptase (Invitrogen, 18064022) following the manufacturer's recommendations. RT-qPCR was performed using the Power SYBR Green Master Mix (Applied Biosystems, 4367659). Transcription analyses were performed using the $2^{-\Delta\Delta Ct}$ method with the mean threshold cycle (Ct) value obtained from three replicates.

Subcutaneous Tumors and In Vivo Treatments. KP or KL tumor-derived cell lines with C57BL/6JOlaHsd genetic background were transduced with a tetracycline-inducible system, either as an empty vector (pLVX-TetOne-Puro; Takara Bio, 631849) or to express IFN-β (pLVX-TetOne-*Ifnb1*-Puro) or STING^{V154M} (pLVX-TetOne-*Sting1-V154M*-Puro). Cells were cultured in DMEM supplemented with 10% tetracycline-free FBS (Biowest, S181T-500). 500,000 cells prepared in a suspension of 1:1 mixture of PBS and Matrigel (Corning, 354234) were subcutaneously injected in both flanks of either 8 to 10 wk old C57BL/6JOlaHsd or immunocompromised Foxn1$^{nu/nu}$ animals (Envigo). When the tumors reached volumes between 100 and 200 mm^3, the mice were fed ad libitum with a doxycycline hyclate-containing diet (SAFE U8978 v.168, AIN93G 2 g/kg Doxycycline Hyclate supplemented custom diet) until the end of the corresponding experiments. For the treatments, 12.5 mg/kg of IgG2a isotype control (ISO, Bio X Cell, *InVivo*MAb, BE0089) or anti-mouse-PD-1 (α-PD-1, Bio X Cell, *InVivo*MAb, BE0146) antibodies were administered twice per week. Tumor volumes were monitored three times per week by caliper measurements. Tumor volume (V) was calculated using the formula V = (π/6)×(length×width×height).

Characterization of Intratumoral Immune Cell Populations. After 14 d of doxycycline administration the subcutaneous tumors from C57BL/6JOlaHsd mice were minced using scalpels and enzymatically digested (1 mg/mL Collagenase IV [Gibco, 17104019), 0.1 mg/mL DNase I (Sigma, DN25) in HBSS] at 37 °C for 30 min. The samples were washed with cold FACS buffer (1% BSA, 2 mM EDTA in PBS) and the erythrocytes were lysed using the buffer EL (Qiagen, 79217) on ice for 10 min. Fc receptors were blocked with anti-mouse CD16/CD32 (BD Pharmingen, 553142). Cells were stained on ice for 45 min using the following antibodies: CD45-FITC (BD Pharmigen, 553080); CD3e-APC (BD Pharmigen, 553066); CD4-PerCP-Cy5.5 (BD Pharmigen, 550954); CD8a-PE-Cy7 (BD Pharmigen, 552877); CD49b-PE (BD Pharmigen, 553858); CD11b-PE-Cy7 (BD Bioscience, 552850); Ly-6C-BV421 (BioLegend, 128031); Ly-6G-APC (BioLegend, 127613); F4/80-PE (eBioscience, 12-4801-82); CD11c-BUV737 (BD Bioscience, 612797); MHC-II (I-A/I-E)-BV786 (BD Bioscience, 742894). Zombie Violet Fixable Dye (BioLegend, 423114) and Zombie UV Fixable Dye (BioLegend, 423108) viability dyes were used. The PFA fixed stained samples were analyzed by multicolor immunophenotyping using the FACSCanto II or LSRFortessa cytometers. UltraComp eBeads™ Compensation beads were used for flow cytometry compensation. The data were analyzed using FlowJo 10.8.1.

Statistical Analyses. Normality of the data was assessed by using the D'Agostino–Pearson omnibus test. Homogeneity of variance was evaluated in normal data by using the Brown–Forsythe test. Statistical significance was evaluated by one-way or two-way ANOVA followed by Holm–Sidak's multiple comparison post hoc test. Alternatively, a Kruskal–Wallis test followed by a Dunn's multiple comparisons post hoc test were performed. Differences in tumor growth of subcutaneous tumors were evaluated by first calculating the area under the curve and then performing the Kruskal–Wallis test followed by Dunn's multiple comparisons post hoc test. *P* values are reported as ns for not significant, * for $P < 0.05$, ** for $P < 0.01$, *** for $P < 0.001$, and **** for $P < 0.0001$. Error bars represent the mean ± SEM. All statistic analyses were performed using Prism 8 for macOS Version 8.4.0.

Data, Materials, and Software Availability. The data discussed in this publication have been deposited in NCBI's Gene Expression Omnibus and are accessible through GEO Series accession numbers: GSE274477 (64) (scRNAseq data of KRAS wild type and KRAS mutant AT2 cells), GSE274351 (65) (RNAseq data of K, KP and KL LCM adenoma samples) and GSE274352 (66).

ACKNOWLEDGMENTS. We thank Raquel Villar (Experimental Oncology); Mayte Lamparero, Flora Díaz, and Isabel Blanco (Animal Facility); Lola Martínez (Flow Cytometry Unit); and Eduardo Caleiras (Histopathology Unit) for technical assistance. This work was supported by grants from the European Research Council (ERC-AG/695566, THERACAN) to M.B. and grants from the Spanish Ministry of Science, Innovation and Universities cofounded by the European Regional Development Fund "A way of making Europe": RTI2018-094664-B-I00 to M.B. and M.M. and PID2021-122797OB-I00 to M.M. M.B. is a recipient of an Endowed Chair from the AXA Research Fund. M.M. is recipient of a "Ramón y Cajal" fellowship from the Spanish Ministry of Science, Innovation and Universities. F.F.-G. and A.F.-R. were supported by a Formación de Profesorado Universitario fellowship from the Spanish Ministry of Science, Innovation and Universities.

Author affiliations: [a]Experimental Oncology Group, Molecular Oncology Program, Centro Nacional de Investigaciones Oncológicas, Madrid 28029, Spain; [b]Bioinformatics Unit, Centro Nacional de Investigaciones Oncológicas, Madrid 28029, Spain; [c]School of Life Sciences and Technology, Tongji University, Shanghai 200092, China; [d]Genomic Unit, Centro Nacional de Investigaciones Cardiovasculares, Madrid 28029, Spain; [e]Centro de Investigación Biomédica en Red de Cáncer, Instituto de Salud Carlos III, Madrid 28029, Spain; [f]Department of Molecular Biotechnology and Health Sciences, Molecular Biotechnology Center, University of Torino, Torino 10126, Italy; [g]Molecular Mechanisms of Cancer Program, Centro de Investigación del Cáncer, Consejo Superior de Investigaciones Científicas-Universidad de Salamanca, Salamanca 37007, Spain; [h]Centro de Investigación Biomédica en Red de Enfermedades Cardiovasculares, Instituto de Salud Carlos III, Madrid 28029, Spain; [i]Department of Biochemistry and Molecular Biology, Faculty of Pharmacy, Complutense University of Madrid, Madrid 28040, Spain; and [j]Cancer and Obesity Group, Health Research Institute of San Carlos, Madrid 28040, Spain

1. V. W. Chen *et al.*, Analysis of stage and clinical/prognostic factors for lung cancer from SEER registries: AJCC staging and collaborative stage data collection system. *Cancer* **120** (suppl. 23), 3781–3792 (2014).
2. Y. H. Luo *et al.*, 5-year overall survival in patients with lung cancer eligible or ineligible for screening according to US Preventive Services Task Force criteria: A prospective, observational cohort study. *Lancet Oncol.* **20**, 1098–1108 (2019).
3. P. Goldstraw *et al.*, The IASLC lung cancer staging project: Proposals for revision of the TNM stage groupings in the forthcoming (eighth) edition of the TNM classification for lung cancer. *J. Thorac. Oncol.* **11**, 39–51 (2016).
4. I. Z. Uras, H. P. Moll, E. Casanova, Targeting KRAS mutant non-small-cell lung cancer: Past, present and future. *Int. J. Mol. Sci.* **21**, 4325 (2020).

5. M. Drosten, M. Barbacid, Targeting KRAS mutant lung cancer: Light at the end of the tunnel. *Mol. Oncol.* **16**, 1057–1071 (2022).
6. J. Canon *et al.*, The clinical KRAS(G12C) inhibitor AMG 510 drives anti-tumour immunity. *Nature* **575**, 217–223 (2019).
7. D. S. Hong *et al.*, KRAS(G12C) inhibition with sotorasib in advanced solid tumors. *N. Engl. J. Med.* **383**, 1207–1217 (2020).
8. P. A. Janne *et al.*, Adagrasib in non-small-cell lung cancer harboring a KRAS(G12C) mutation. *N. Engl. J. Med.* **387**, 120–131 (2022).
9. M. M. Awad *et al.*, Acquired resistance to KRAS(G12C) inhibition in cancer. *N. Engl. J. Med.* **384**, 2382–2393 (2021).
10. A. J. de Langen *et al.*, Sotorasib versus docetaxel for previously treated non-small-cell lung cancer with KRAS(G12C) mutation: A randomised, open-label, phase 3 trial. *Lancet* **401**, 733–746 (2023).
11. M. Molina-Arcas, J. Downward, Exploiting the therapeutic implications of KRAS inhibition on tumor immunity. *Cancer Cell* **42**, 338–357 (2024).
12. D. Kim *et al.*, Pan-KRAS inhibitor disables oncogenic signalling and tumour growth. *Nature* **619**, 160–166 (2023), 10.1038/s41586-023-06123-3.
13. X. Wang *et al.*, Identification of MRTX1133, a noncovalent, potent, and selective KRAS(G12D) inhibitor. *J. Med. Chem.* **65**, 3123–3133 (2022).
14. A. D. Waldman, J. M. Fritz, M. J. Lenardo, A guide to cancer immunotherapy: From T cell basic science to clinical practice. *Nat. Rev. Immunol.* **20**, 651–668 (2020).
15. L. Gandhi *et al.*, Pembrolizumab plus chemotherapy in metastatic non-small-cell lung cancer. *N. Engl. J. Med.* **378**, 2078–2092 (2018).
16. L. G. Paz-Ares *et al.*, First-line nivolumab plus ipilimumab in advanced NSCLC: 4-year outcomes from the randomized, open-label, phase 3 CheckMate 227 part 1 trial. *J. Thorac. Oncol.* **17**, 289–308 (2022).
17. S. Gettinger *et al.*, Five-year follow-up of nivolumab in previously treated advanced non-small-cell lung cancer: Results from the CA209-003 study. *J. Clin. Oncol.* **36**, 1675–1684 (2018).
18. L. Gianoncelli *et al.*, Efficacy of anti-PD1/PD-L1 therapy (IO) in KRAS mutant non-small cell lung cancer patients: A retrospective analysis. *Anticancer Res.* **40**, 427–433 (2020).
19. D. Kauffmann-Guerrero *et al.*, Response to checkpoint inhibition in non-small cell lung cancer with molecular driver alterations. *Oncol. Res. Treat* **43**, 289–298 (2020).
20. F. Skoulidis, J. V. Heymach, Co-occurring genomic alterations in non-small-cell lung cancer biology and therapy. *Nat. Rev. Cancer* **19**, 495–509 (2019).
21. S. Mainardi *et al.*, Identification of cancer initiating cells in K-Ras driven lung adenocarcinoma. *Proc. Natl. Acad. Sci. U.S.A.* **111**, 255–260 (2014).
22. J. Sainz de Aja, A. F. M. Dost, C. F. Kim, Alveolar progenitor cells and the origin of lung cancer. *J. Intern. Med.* **289**, 629–635 (2021).
23. J. E. Wosen, D. Mukhopadhyay, C. Macaubas, E. D. Mellins, Epithelial MHC class II expression and its role in antigen presentation in the gastrointestinal and respiratory tracts. *Front. Immunol.* **9**, 2144 (2018).
24. M. Agassandian, R. K. Mallampalli, Surfactant phospholipid metabolism. *Biochim. Biophys. Acta* **1831**, 612–625 (2013).
25. A. F. M. Dost *et al.*, Organoids model transcriptional hallmarks of oncogenic KRAS activation in lung epithelial progenitor cells. *Cell Stem Cell* **27**, 663–678.e8 (2020).
26. N. D. Marjanovic *et al.*, Emergence of a high-plasticity cell state during lung cancer evolution. *Cancer Cell* **38**, 229–246. e13 (2020).
27. L. W. Gonzales, S. H. Guttentag, K. C. Wade, A. D. Postle, P. L. Ballard, Differentiation of human pulmonary type II cells in vitro by glucocorticoid plus cAMP. *Am. J. Physiol. Lung Cell Mol. Physiol.* **283**, L940–L951 (2002).
28. M. Motwani *et al.*, Hierarchy of clinical manifestations in SAVI N153S and V154M mouse models. *Proc. Natl. Acad. Sci. U.S.A.* **116**, 7941–7950 (2019).
29. M. Motwani, S. Pesiridis, K. A. Fitzgerald, DNA sensing by the cGAS-STING pathway in health and disease. *Nat. Rev. Genet.* **20**, 657–674 (2019).
30. A. Garcia-Diaz *et al.*, Interferon receptor signaling pathways regulating PD-L1 and PD-L2 expression. *Cell Rep.* **19**, 1189–1201 (2017).
31. S. Maleki Vareki, High and low mutational burden tumors versus immunologically hot and cold tumors and response to immune checkpoint inhibitors. *J. Immunother. Cancer* **6**, 157 (2018).
32. M. Jamal-Hanjani *et al.*, Tracking the evolution of non-small-cell lung cancer. *N. Engl. J. Med.* **376**, 2109–2121 (2017).
33. N. Andor *et al.*, Pan-cancer analysis of the extent and consequences of intratumor heterogeneity. *Nat. Med.* **22**, 105–113 (2016).
34. G. Ferone, M. C. Lee, J. Sage, A. Berns, Cells of origin of lung cancers: Lessons from mouse studies. *Genes Dev.* **34**, 1017–1032 (2020).
35. Z. Wang *et al.*, Deciphering cell lineage specification of human lung adenocarcinoma with single-cell RNA sequencing. *Nat. Commun.* **12**, 6500 (2021).
36. N. AbuSara *et al.*, Restoration of IRF1-dependent anticancer effects by MEK inhibition in human cancer cells. *Cancer Lett.* **357**, 575–581 (2015).
37. Y. Komatsu *et al.*, Oncogenic Ras inhibits IRF1 to promote viral oncolysis. *Oncogene* **34**, 3985–3993 (2015).
38. L. Klampfer *et al.*, Oncogenic Ki-ras inhibits the expression of interferon-responsive genes through inhibition of STAT1 and STAT2 expression. *J. Biol. Chem.* **278**, 46278–46287 (2003).
39. W. Liao *et al.*, KRAS-IRF2 axis drives immune suppression and immune therapy resistance in colorectal cancer. *Cancer Cell* **35**, 559–572.e7 (2019).
40. Q. Zhang *et al.*, Activation of the Ras/Raf/MEK pathway facilitates hepatitis C virus replication via attenuation of the interferon-JAK-STAT pathway. *J. Virol.* **86**, 1544–1554 (2012).
41. S. L. Christian *et al.*, Suppression of IFN-induced transcription underlies IFN defects generated by activated Ras/MEK in human cancer cells. *PLoS One* **7**, e44267 (2012).
42. M. Shmulevitz, L. Z. Pan, K. Garant, D. Pan, P. W. Lee, Oncogenic Ras promotes reovirus spread by suppressing IFN-beta production through negative regulation of RIG-I signaling. *Cancer Res.* **70**, 4912–4921 (2010).
43. E. Mugarza *et al.*, Therapeutic KRAS(G12C) inhibition drives effective interferon-mediated antitumor immunity in immunogenic lung cancers. *Sci. Adv.* **8**, eabm8780 (2022).
44. N. Muthalagu *et al.*, Repression of the type I interferon pathway underlies MYC- and KRAS-dependent evasion of NK and B cells in pancreatic ductal adenocarcinoma. *Cancer Discov.* **10**, 872–887 (2020).
45. F. M. Barriga *et al.*, MACHETE identifies interferon-encompassing chromosome 9p21.3 deletions as mediators of immune evasion and metastasis. *Nat. Cancer* **3**, 1367–1385 (2022).
46. A. J. Ozga, M. T. Chow, A. D. Luster, Chemokines and the immune response to cancer. *Immunity* **54**, 859–874 (2021).
47. M. Gu, T. Xu, P. Chang, KRAS/LKB1 and KRAS/TP53 co-mutations create divergent immune signatures in lung adenocarcinomas. *Ther. Adv. Med. Oncol.* **13**, 17588359211006950 (2021).
48. F. Skoulidis *et al.*, Co-occurring genomic alterations define major subsets of KRAS-mutant lung adenocarcinoma with distinct biology, immune profiles, and therapeutic vulnerabilities. *Cancer Discov.* **5**, 860–877 (2015).
49. F. Skoulidis *et al.*, STK11/LKB1 mutations and PD-1 inhibitor resistance in KRAS-mutant lung adenocarcinoma. *Cancer Discov.* **8**, 822–835 (2018).
50. D. G. McFadden *et al.*, Mutational landscape of EGFR-, MYC-, and Kras-driven genetically engineered mouse models of lung adenocarcinoma. *Proc. Natl. Acad. Sci. U.S.A.* **113**, E6409–E6417 (2016).
51. S. Hervas-Stubbs *et al.*, Direct effects of type I interferons on cells of the immune system. *Clin. Cancer Res.* **17**, 2619–2627 (2011).
52. A. R. Sanchez-Paulete *et al.*, Antigen cross-presentation and T-cell cross-priming in cancer immunology and immunotherapy. *Ann. Oncol.* **28**, xii44–xii55 (2017).
53. S. Kitajima *et al.*, Suppression of STING associated with LKB1 loss in KRAS-driven lung cancer. *Cancer Discov.* **9**, 34–45 (2019).
54. A. S. Nagaraj *et al.*, Cell of origin links histotype spectrum to immune microenvironment diversity in non-small-cell lung cancer driven by mutant Kras and loss of Lkb1. *Cell Rep.* **18**, 673–684 (2017).
55. K. G. Mitchell *et al.*, Neutrophil expansion defines an immunoinhibitory peripheral and intratumoral inflammatory milieu in resected non-small cell lung cancer: A descriptive analysis of a prospectively immunoprofiled cohort. *J. Immunother. Cancer* **8**, e000405 (2020).
56. M. Chawla-Sarkar *et al.*, Apoptosis and interferons: Role of interferon-stimulated genes as mediators of apoptosis. *Apoptosis* **8**, 237–249 (2003).
57. A. Takaoka *et al.*, Integration of interferon-alpha/beta signalling to p53 responses in tumour suppression and antiviral defence. *Nature* **424**, 516–523 (2003).
58. J. Boumelha *et al.*, An immunogenic model of KRAS-mutant lung cancer enables evaluation of targeted therapy and immunotherapy combinations. *Cancer Res.* **82**, 3435–3448 (2022).
59. S. Marino, M. Vooijs, H. van Der Gulden, J. Jonkers, A. Berns, Induction of medulloblastomas in p53-null mutant mice by somatic inactivation of Rb in the external granular layer cells of the cerebellum. *Genes Dev.* **14**, 994–1004 (2000).
60. D. Nakada, T. L. Saunders, S. J. Morrison, Lkb1 regulates cell cycle and energy metabolism in haematopoietic stem cells. *Nature* **468**, 653–658 (2010).
61. S. Srinivas *et al.*, Cre reporter strains produced by targeted insertion of EYFP and ECFP into the ROSA26 locus. *BMC Dev. Biol.* **1**, 4 (2001).
62. C. Guerra *et al.*, Tumor induction by an endogenous K-ras oncogene is highly dependent on cellular context. *Cancer Cell* **4**, 111–120 (2003).
63. K. Hasegawa *et al.*, Fraction of MHCII and EpCAM expression characterizes distal lung epithelial cells for alveolar type 2 cell isolation. *Respir. Res.* **18**, 150 (2017).
64. F. Fernández-García *et al.*, Type I interferon signaling pathway enhances immune-checkpoint inhibition in KRAS mutant lung tumors [scRNA-seq]. NCBI GEO database. https://www.ncbi.nlm.nih.gov/geo/query/acc.cgi?acc=GSE274477. Deposited 2 August 2024.
65. F. Fernández-García *et al.*, Type I interferon signaling pathway enhances immune-checkpoint inhibition in KRAS mutant lung tumors [LCM]. NCBI GEO database. https://www.ncbi.nlm.nih.gov/geo/query/acc.cgi?acc=GSE274351. Deposited 2 August 2024.
66. F. Fernández-García *et al.*, Type I interferon signaling pathway enhances immune-checkpoint inhibition in KRAS mutant lung tumors [cell lines]. NCBI GEO database. https://www.ncbi.nlm.nih.gov/geo/query/acc.cgi?acc=GSE274352. Deposited 2 August 2024.